Non-modal transient growth of disturbances in pulsatile and oscillatory pipe flow

Preprint · August 2020

CITATIONS
0

READS
103

3 authors:

Duo Xu
Friedrich-Alexander-University of Erlangen-Nürnberg
17 PUBLICATIONS **120** CITATIONS
SEE PROFILE

Baofang Song
Tianjin University
17 PUBLICATIONS **214** CITATIONS
SEE PROFILE

Marc Avila
Universität Bremen
71 PUBLICATIONS **1,621** CITATIONS
SEE PROFILE

Non-modal transient growth of disturbances in pulsatile and oscillatory pipe flow

Duo Xu[1]†, Baofang Song[2] and Marc Avila[1]

[1] University of Bremen, Center of Applied Space Technology and Microgravity (ZARM), 28359 Bremen, Germany

[2] Tianjin University, Center for Applied Mathematics, Tianjin 300072, China

(Received ?; revised ?; accepted ?. - To be entered by editorial office)

Laminar flows through pipes driven at steady, pulsatile or oscillatory rates undergo a sub-critical transition to turbulence. We carry out an extensive linear non-modal stability analysis of these flows and show that for sufficiently high pulsation amplitudes the streamwise vortices of the classic lift-up mechanism are outperformed by helical disturbances exhibiting an Orr-like mechanism. In oscillatory flow, the energy amplification depends solely on the Reynolds number based on the Stokes-layer thickness and for sufficiently high oscillation frequency and Reynolds number, axisymmetric disturbances dominate. In the high-frequency limit, these axisymmetric disturbances are exactly similar to those recently identified by Biau (2016) for oscillatory flow over a flat plate. In all regimes of pulsatile and oscillatory pipe flow, the optimal helical and axisymmetric disturbances are triggered in the deceleration phase and reach their peaks in typically less than a period. Their maximum energy gain scales exponentially with Reynolds number of the oscillatory flow component. Our numerical computations unveil a plausible mechanism for the turbulence observed experimentally in pulsatile and oscillatory pipe flow.

Key words:

1. Introduction

Physiological flows are unsteady in nature and are characterized by complex geometries and fluid-structure interaction. In healthy individuals, arterial flow is generally assumed laminar, but complex (*disturbed*) flow patterns are acknowledged to play an important mechanistic role in the development of vascular diseases (Ku 1997; Chiu & Chien 2011). Even for the simple case of pulsatile flow in a straight pipe, the mechanisms of instability and transition to turbulence are poorly understood and particularly the dependence on the pulsation amplitude ($A = U_o/U_s$, where U_o and U_s are the magnitude of the oscillatory and steady components of the velocity) is largely unknown. This makes it difficult to assess whether disturbed flow patterns in arterial and respiratory flow are solely due to geometric and structural effects (e.g. vessel curvature and flexibility, bifurcations), or are also related to the stability of pulsatile pipe flow.

Pulsatile flow in a straight pipe is governed by the pulsation amplitude A, the Wommersly number $Wo = D/2\sqrt{\omega/\nu}$ and the Reynolds number $Re_s = U_s D/\nu$. Here D the pipe diameter, ω the angular frequency of the pulsation and ν the kinematic viscosity of the fluid. The limit of small pulsation amplitude $A \to 0$ (steady flow), is relevant to

† Email address for correspondence: duo.xu@zarm.uni-bremen.de

laminar blood flow in capillaries, whereas the opposite limit $A \to \infty$ (oscillatory flow) is relevant to respiratory flow. In humans, the airflow may be laminar, transitional or turbulent depending on the airway segment (Kleinstreuer & Zhang 2010). The intermediate regime, in which the pulsatile flow component is similar to the steady one ($A \gtrsim 1$), is typical of blood flow in the large arteries. This regime has received little attention in studies of pulsatile pipe flow.

Steady laminar pipe flow is linearly stable and transition can only be triggered with finite-amplitude disturbances (Reynolds 1883). Following transition, turbulence persists provided that $Re_s \gtrsim 2040$ (see Avila *et al.* 2011). Despite the non-linear nature of the transition, the key underlying mechanism is linear (Schmid & Henningson 2001). The Navier–Stokes equations linearized about the laminar flow are non-normal and disturbances can be transiently amplified before asymptotically decaying. Schmid & Henningson (1994) showed that in pipe flow the optimal (non-modal) disturbance consists of a pair of stream-wise rolls, which generate a pair of stream-wise velocity streaks (lift-up mechanism). The perturbation's energy gain in this process scales as $G \propto Re_s^2$, and keeping the flow laminar as Re_s increases becomes an arduous task.

Oscillatory pipe flow is linearly (Floquet) unstable when the Reynolds number based on the Stokes-layer thickness, $Re_\delta = U_o\delta/\nu \gtrsim 10^3$, where $\delta = \sqrt{2\nu/\omega}$ is the thickness of the Stokes layer (Thomas *et al.* 2012). In experiments turbulence was observed already for $280 \lesssim Re_\delta \lesssim 550$ (Sergeev 1966; Merkli & Thomann 1975; Hino *et al.* 1976; Eckmann & Grotberg 1991; Zhao & Cheng 1996), indicating that oscillatory pipe flow also undergoes transition via finite-amplitude disturbances. Feldmann & Wagner (2012, 2016) performed direct numerical simulations of oscillatory pipe flow initialized with fully turbulent fields and confirmed the existence of sustained turbulence in the sub-critical regime. Thomas *et al.* (2011) showed that the linear instability of oscillatory pipe flow persists also for pulsatile flow, however in experiments transition occurs much earlier than predicted by linear analysis (e.g., Sarpkaya 1966; Stettler & Hussain 1986; Xu *et al.* 2017, 2020). Taken together these results suggest that pulsatile pipe flow undergoes a sub-critical transition to turbulence in all regimes (including the limiting cases of steady and oscillatory driving).

Xu *et al.* (2020) recently reported on a nonlinear instability of pulsatile pipe flow, which occurs at pulsation amplitudes relevant for arterial flow. In their experiments, geometric imperfections triggered a helical wave pattern which emerged cyclically during the deceleration phase and broke down into turbulence, before decaying. For $A = 1$ they observed transition at Reynolds numbers as low as $Re_s \approx 800$. In addition, Xu *et al.* (2020) performed also linear non-modal transient growth computations at a selected parameter set and showed that the most amplified disturbance was a helical wave. Direct numerical simulations initialized with this helical wave reproduced the flow patterns and the time of turbulence breakdown observed experimentally, which suggests an important role of transient growth in pulsatile flows. Large non-modal transient amplification of disturbances has also been found in pulsatile channel flow $5 \leqslant Wo \leqslant 50$ (Tsigklifis & Lucey 2017) and in the two-dimensional Stokes layer over an oscillatory flat plate (Biau 2016), where phase-dependent energy growth increases exponentially with Re_δ. In what follows, we present a comprehensive non-modal linear analysis of the sub-critical regimes of pulsatile and oscillatory pipe flows.

2. Methods

We consider an incompressible viscous fluid driven at a pulsatile flow rate in a straight pipe of circular cross-section. Lengths, velocities and time are rendered dimensionless

with D, U_s and D/U_s, respectively. The dimensionless fluid velocity averaged over the circular cross-section reads

$$U(t) = U_s \cdot [1 + A \cdot \sin(2\pi \cdot t/T)], \tag{2.1}$$

where $T = \pi Re_s/(2\,Wo^2)$ is the dimensionless pulsation period. (In oscillatory flow, lengths, velocities and time are rendered dimensionless with D, U_o and D/U_o, respectively.) The linearized Navier–Stokes equations (and their adjoint) are discretized in cylindrical coordinates (r, θ, z) with a Chebyshev collocation method for each Fourier mode (k, m), where k and m are the axial and azimuthal wavenumbers of the perturbation, respectively. A second-order projection scheme was used to integrate the equations in time (see Xu *et al.* 2020, for details of the method). We used a time steps down to $\Delta t = 0.002$ and $N = 96$ radial points (convergence was checked at selected parameter values with $\Delta t = 0.0005$ and $N = 128$). The optimal transient energy growth of a disturbance $\mathbf{u'}_{km}$ with wavenumbers (k, m) was computed as

$$G_{km}(t_0, \tau) = \max_{||\mathbf{u'}_{km}(t_0)||_2 \neq 0} \frac{E_{km}(t_0 + \tau)}{E_{km}(t_0)}, \tag{2.2}$$

with the adjoint method of Barkley *et al.* (2008). Here $E_{km}(t)$ is the kinetic energy of the disturbance at time t, t_0 the time (phase) at which the perturbation is applied and t_f the point at which the growth is evaluated ($\tau = t_f - t_0$ is the perturbation evolution time). We varied Re_s, A, and Wo independently and for each set of parameter values the maximum transient growth $G_{\max}$ was optimized over t_0, τ, k and m. We found that in most regimes the optimal azimuthal wavenumber is $m = 1$ (except for some regimes of oscillatory flow). In all the results shown below $m = 1$ unless otherwise specified.

3. Dynamics of the optimal disturbance

The temporal evolution of the optimal disturbance's energy at $Re_s = 2000$, $A = 1$ and $Wo = 15$ is shown as a dashed line in figure 1(a). At these parameter values the optimal disturbance has a helical structure with $(k, m) = (3.24, 1)$ and is localized at the outer half of the pipe (exceeding the Stokes layer thickness), see figure 1(f)–(g). The optimal point to disturb is during the deceleration phase, at $t_0/T = 0.5$, whereas the maximum amplification is reached during the acceleration phase, at $t_f/T = 1.2$. The classic $k = 0$, $m = 1$ optimal disturbance of steady pipe flow is also amplified significantly in this case, albeit an order of magnitude less than the helical one. The classic disturbance initially consists of stream-wise vortices, as shown in figure 1(d)–(e), and the energy is subsequently transferred to the stream-wise velocity components, while the cross-stream components decay monotonically, see figure 1(b) and supplementary movie 1. Overall the classic perturbation's behavior appears to be rather insensitive to the change in flow profile throughout the cycle and the decay is very slow. By contrast, the kinetic energy of the optimal helical perturbation is mostly distributed in the stream-wise and azimuthal components, which self-amplify rapidly during the deceleration phase and a bit slower during the subsequent acceleration phase, see figure 1(c). Initially the disturbance spirals clock-wisely towards the pipe center while leaning against the background shear profile, see figure 1(f) and supplementary movie 2. As the energy grows, the perturbation switches the spiraling direction and is tilted by the shear until it aligns with it and the disturbance finally decays, see figure 1(g). This is reminiscent of the Orr mechanism (Orr 1907). However, approximately 96% of the kinetic energy is shared in equal parts between the azimuthal and stream-wise components, which indicates a strong three-dimensional

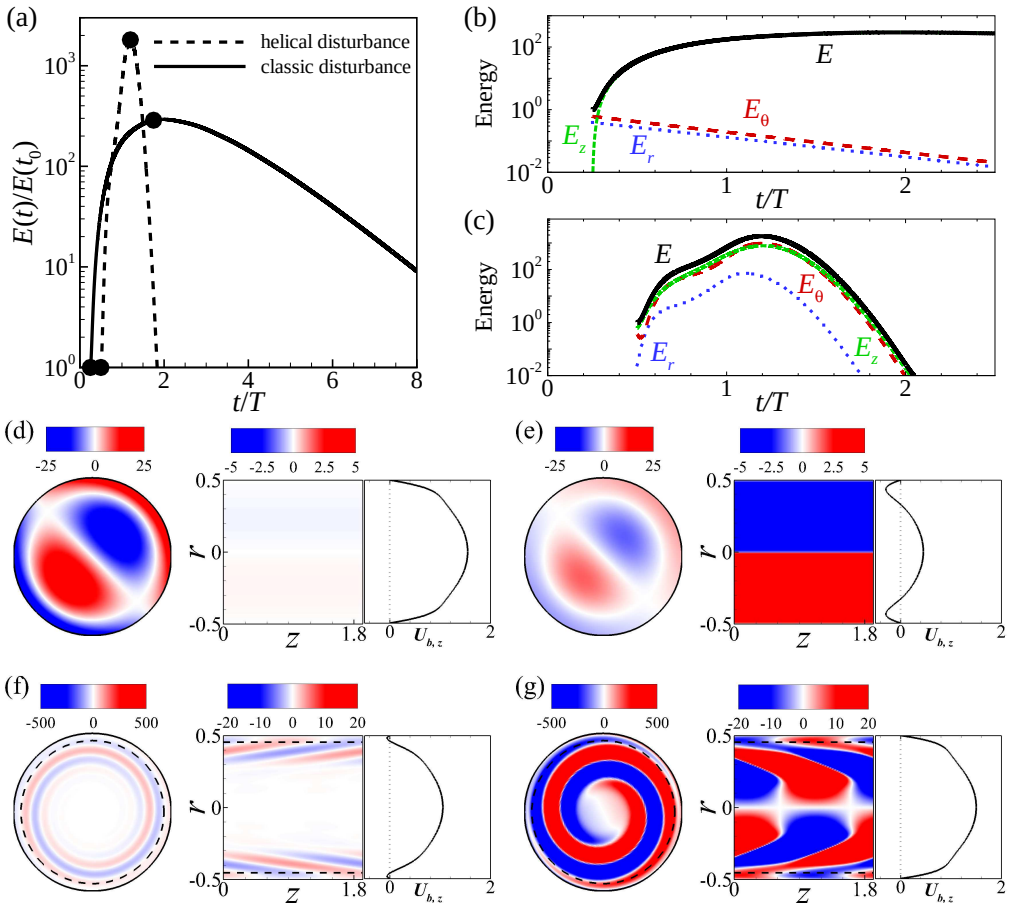

Figure 1: (a) Time series of the kinetic energy $E(t)/E(t_0)$ of the optimal helical, $(k, m) = (3.24, 1)$, and classic, $(k, m) = (0, 1)$, disturbances at $(Re_s, A, Wo) = (2000, 1, 15)$. (b)–(c) Time series of kinetic energy contribution of each velocity component for the classic (b) and helical (c) disturbances. (d)–(e) Contours of stream-wise vorticity (on a r-θ cross-section) and of stream-wise velocity (on a z-r cross-section) of the classic disturbance, and the corresponding base flow profile $\boldsymbol{U}_{b,z}$ at $t_0/T = 0.25$ (d) and $t_f/T = 1.75$; see supplementary movie 1 for an animation of the disturbance dynamics (e). (f)–(g) The same as (d)–(e), but for the helical disturbance at $t_0/T = 0.5$ and $t_f/T = 1.2$; see also supplementary movie 2. The dashed line denotes the Stokes-layer thickness.

effect, distinct from the two-dimensional Orr mechanism reported for many flows (see e.g. Boyd 1983; Farrell 1988; Schmid & Henningson 2001; Maretzke *et al.* 2014; Biau 2016).

The black thick line in figure 2(a) depicts the maximum energy amplification $G(t_f)$ over all (k, m) and initial disturbances time $t = t_0$. The maximum amplification is reached during the acceleration phase via helical disturbances, as shown in figure 2(b), whereas the classic disturbance achieves larger growth only during the second half of the deceleration phase. The colormap of figure 2(c) shows that the optimal time to perturb the flow is during middle of the deceleration phase ($t_0/T \approx 0.5$); perturbing during the acceleration phase leads to much lower growth (yielded by the classic disturbance during the deceleration phase). Clearly the helical mechanism is efficient only in the deceleration phase. The time needed to reach the maximum growth is about $\tau \approx 3/4T$, which explains why the maximum growth occurs during the acceleration phase.

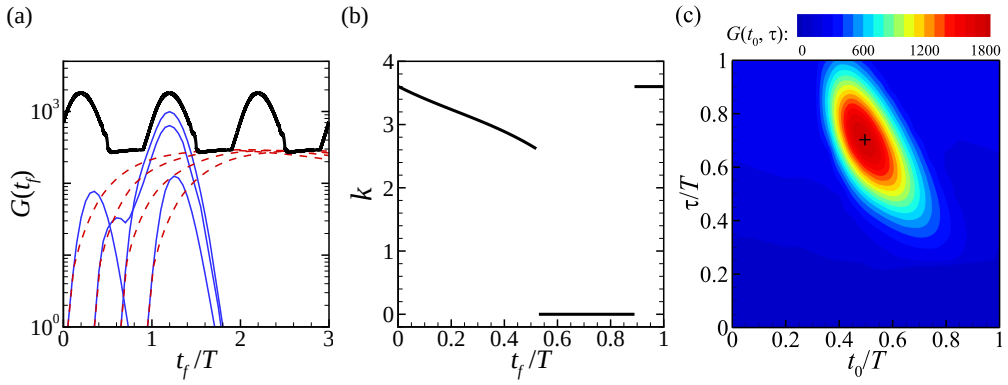

Figure 2: Transient growth at $(Re_s, A, Wo) = (2000, 1, 15)$: (a) The red dashed lines denote the temporal evolution of the optimal classic disturbances $(k, m) = (0, 1)$ for four different initial times t_0, whereas the blue solid lines correspond to the optimal helical disturbances $(k, m) = (3.24, 1)$ initialized at the same t_0. The thick black line is the maximum gain $G(t_f)$ that can be achieved at a given time t_f (optimized over k, m and t_0 disturbances). (b) Dependence of the optimal axial wavenumber k (associated to the thick line of a) on t_f. (c) Colormap of the maximum gain $G(t_0, \tau)$ (optimized over k and m) in the $t_0 - \tau$ plane. The black cross marks the maximum of G.

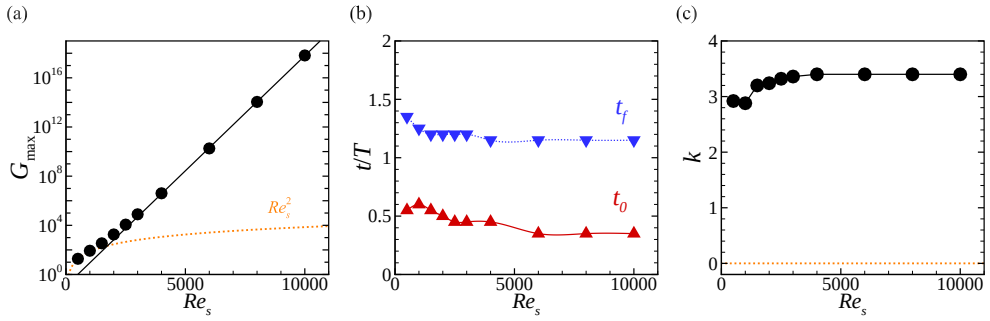

Figure 3: Optimal transient growth as a function of Re_s for $(A, Wo) = (1, 15)$. (a) The symbols show the computed maximum energy gain. The black solid line $G_{\max} = \exp(Re_s/232 - 2.12)$ is a fit to the data for $Re_s \geqslant 4000$. The orange dotted line $G_{\max} = 2.72\, Re_s^2$ is a fit to data for $(A, Wo) = (1, 25)$. (b)–(c) Optimal initial and final disturbance times and axial wavenumber.

4. Parametric study of transient growth

We show in figure 3(a) that keeping $(A, Wo) = (1, 15)$ fixed and increasing the Reynolds number leads to an approximately exponential increase of the energy gain $G_{\max}$. This is as reported for the oscillatory Stokes layer over a flat plate (Biau 2016) and for the flow following an axisymmetric stenosis (Blackburn *et al.* 2008). Independently of the Reynolds number, the maximum energy amplification occurs always during flow acceleration with helical disturbances introduced during the deceleration phase, see figure 3(b). As shown in figure 3(c) an asymptotic behavior is approached for $Re_s \gtrsim 5000$, with $k \approx 3.4$, $t_f/T \approx 1.15$ and $t_0/T \approx 0.35$.

The effect of the pulsation amplitude A, whilst keeping $(Re_s, Wo) = (2000, 15)$ fixed is illustrated in figure 4. For steady pipe flow ($A = 0$), Meseguer & Trefethen (2003) obtained $G_{\max} \approx 288.7$, $\tau \approx 24.5$ and $(k, m) = (0, 1)$, which is in line with our results were for pulsatile flow of low amplitude $A \lesssim 0.55$. Helical disturbances dominate thereafter, but their energy gain does not grow monotonically (exponentially) with the amplitude

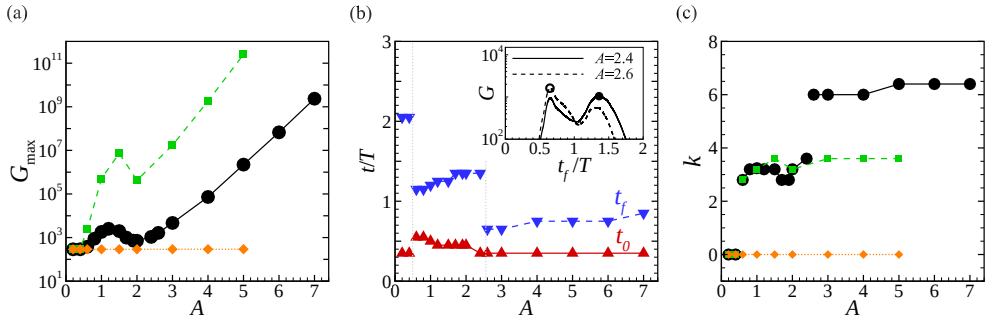

Figure 4: Optimal transient growth as a function of A for $(Re_s, Wo) = (2000, 15)$. (a) The black circles show the computed maximum energy gain, the green squares and the orange diamonds are for $(Re_s, Wo) = (2000, 10)$ and $(Re_s, Wo) = (2000, 20)$, respectively. (b)–(c) Optimal initial and final disturbance times and axial wavenumber. The maximum gain as a function of t_f/T is shown in the inset in (b) for $A = 2.4$ and 2.6 and illustrates the competition between two distinct different disturbances.

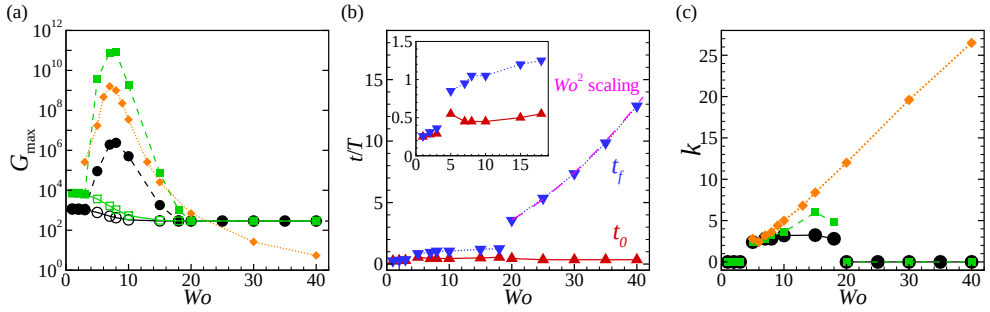

Figure 5: Effect of the Wommersly number Wo on the transient growth. (a) Maximum energy gain for $(Re_s, A) = (2000, 1)$ (black circles), $(Re_s, A) = (2000, 4)$ (green squares) and oscillatory flow at $Re_o = 8000$ $(Re_s, A) = (0, \infty)$ (orange diamonds). The hollow symbols show the optimal growth of classic disturbances $(k, m) = (0, 1)$ in the regime where the helical disturbance domiates. (b) Optimal initial and final disturbance times at $(Re_s, A) = (2000, 1)$. The pink dashed line shows $t_f/T = (\tau_{\text{steady}} + t_0)/T$, where τ_{steady} is the optimal evolution time of the classic disturbance in steady pipe flow at $Re_s = 2000$. The inset shows a zoom the data for $Wo \lesssim 18$. (c) Optimal axial wavenumber.

until $A \gtrsim 4$. For intermediate amplitudes there is competition between two distinct types of helical disturbances, as shown in figures 4(b). For $0.55 \lesssim A \lesssim 2.5$, the dominant helical disturbance is similar to that examined in detail in figures 2–3, whereas for $A \gtrsim 2.5$ another helical disturbance, with much shorter axial length and shorter evolution time $\tau = t_f - t_0$, takes over. Both types of helical disturbances are triggered in the deceleration phase. Similar results were obtained for lower frequency, at $(Re_s, Wo) = (2000, 10)$, see the green lines in figures 4(a) and (c). Here the maximum growth G is over two orders of magnitude larger and helical disturbances dominate earlier (already for $A \gtrsim 0.41$). From the data in figures 3(a) and 4(a) we conclude that the maximum energy gain of helical disturbances scales exponentially with the Reynolds number of the oscillatory flow component $Re_o = U_o D/\nu = A Re_s$.

In what follows we examine the influence of the pulsation frequency on the dominant mechanism of transient growth in more detail. We begin by focusing on $Re_s = 2000$ and $A = 1$. The circles in figure 5(a) show that for sufficiently large $Wo \gtrsim 20$ the classic disturbance dominates and the optimal gain G of steady pipe flow is recovered (exactly

as for the data shown as a orange lines in figures 3 and 4). As shown in figure 5(b), the perturbation growth time $\tau \approx 25$ is also indistinguishable from that of steady pipe flow. It can be concluded that in the limit $Wo \to \infty$ the disturbance response is solely governed by Re_s. The dynamics of the steady pipe flow is also recovered in the quasi-steady limit $Wo \to 0$, where the classic perturbation dominates as well. In this limit, the maximum transient growth is governed by the maximum Reynolds number $Re_{\max} = (1 + A)Re_s = Re_s + Re_o$ and occurs for $t_0, t_f \to T/4$, see the inset in figure 5(b). For instance, for $Re_s = 2000$, $A = 1$ and $Wo = 3$ the maximum gain is $G \approx 1100$, which is slightly less than the gain for steady pipe flow $G \approx 1155$ at $Re_s = 4000$ (Meseguer & Trefethen 2003). As shown in figure 5(c), helical disturbances dominate for intermediate $4 \lesssim Wo \lesssim 18$ and exhibit a sharp maximum in gain at $Wo \approx 7$, figure 5(a). The results for $A = 4$ (shown in figure 5a as green squares) are qualitatively similar to those for $A = 1$, but the energy gain is much larger.

5. Transient growth in oscillatory pipe flow

The dependence of the energy gain G on the frequency for the specific case of oscillatory flow at $Re_o = 8000$ is shown as orange diamonds in figure 5(a) and follows the trend of pulsatile flow. In figure 6(a) these data are shown as a function of the Reynolds number of the Stokes layer $Re_\delta = U_o\delta/\nu = Re_o/(\sqrt{2}Wo)$, together with three additional sets for $Wo = 10$, 15 and 20 covering wide ranges of Re_o. At low Re_δ, the maximum gain $G = 1$ is reached for $t_0 = t_f$, implying that all perturbations decay monotonously, and the disturbance with $(k = 0, m = 0)$ is the least damped, see figure 6(b)–(c). This can also be seen in figure 5(a), where the limit $G \to 1$ is reached by the orange data points as $Wo \to 0$ (and hence $Re_\delta \to 0$ for constant $Re_o = 8000$). For $Re_\delta \gtrsim 100$ the energy gain increases exponentially with Re_δ and depends only very weakly on the Wommersly number. All data sets shown in figure 6(a) exhibit excellent collapse, except for the data set at $Re_o = 8000$, which deviates from the exponential scaling for $Re_\delta \gtrsim 630$ (corresponding to $Wo \lesssim 9$, i.e. near and below the peak in figure 5a). The optimal point to disturb the flow is during the deceleration phase at $t_0/T \approx 0.35$ (as in figure 3b at sufficiently high Re_o). The maximum energy gain is attained toward the end of the deceleration phase at low Re_δ, and moves progressively into the acceleration phase as Re_δ increases.

Snapshots of the span-wise vorticity of the optimal perturbation are shown in figure 6(d)–(g) for $Wo = 10$ and $Re_\delta = 530$. Initially, the perturbation leans against the background shear and then tilts to align with the stream-wise direction as it propagates radially inwards (see supplementary movie 3). The helical structure and dynamics of the disturbance are very similar to that shown in figure 1(f), but here the disturbance is initially more confined to the Stokes layer. In figure 6(h)–(k) and supplementary movie 4 we show that at higher $Wo = 15$, the optimal disturbance is very similar in dynamics, but is axisymmetric (see also figure 6(c)). The energy growth occurring here is as in the classic Orr mechanism, with the only difference that the perturbation travels radially inwards as it changes the tilt direction. We stress that despite this difference in the disturbance geometry (helical versus axisymmetric), the energy gain, the point of disturbance and the point of maximum gain are indistinguishable (also for larger $Wo = 20$, see figure 6a–c).

6. Conclusion

The lift-up mechanism, by which kinetic energy is transferred from stream-wise vortices to stream-wise streaks, is well-known to play a key role in turbulence and the transition to

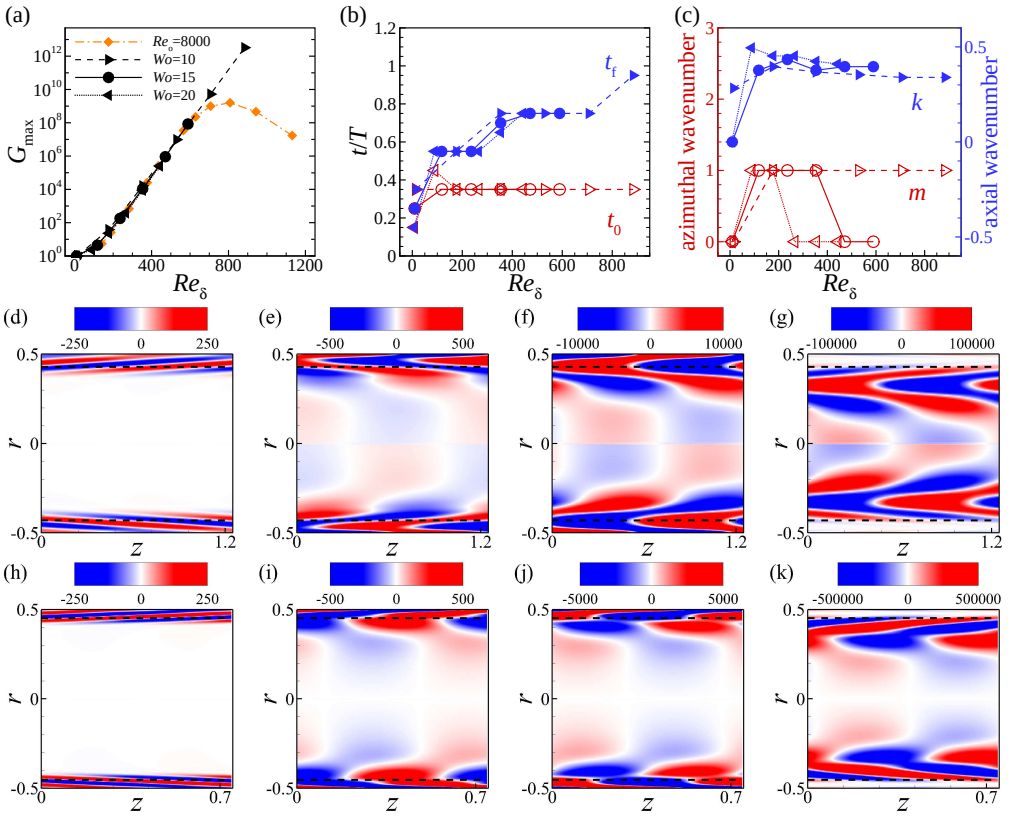

Figure 6: Transient growth of disturbances in oscillatory pipe flow for $Wo = 10$, 15 and 20 as a function of Re_δ: (a) energy amplification, (b)–(c) optimal initial and final disturbance times and optimal wavenumbers, where the axial wavenumber is scaled with δ^{-1}. (d)–(g) Contours of span-wise vorticity (on a $z - r$ cross-section) of the optimal helical disturbance ($m = 1$) for $Wo = 10$ and $Re_\delta = 530$ at $t_0/T = 0.35$ (d), $t/T = 0.4$ (e), $t/T = 0.5$ (f) and $t_f/T = 0.75$ (g); see supplementary movie 3 for an animation. (h)–(k) The same as (d)–(g), but for the optimal axisymmetric disturbance ($m = 0$) for $Wo = 15$ and $Re_\delta = 589$ at $t_0/T = 0.35$ (h), $t/T = 0.4$ (i), $t/T = 0.5$ (j) and $t_f/T = 0.75$ (k); see supplementary movie 4.

turbulence in wall-bounded shear flows (see e.g. Brandt 2014). Here we showed that the lift-up mechanism (classic disturbance) produces the largest transient growth in pulsatile flow of low amplitude, $A \lesssim 0.4$. This is in agreement with recent experiments of Xu *et al.* (2017) and direct numerical simulations of Xu & Avila (2018), exhibiting turbulent puff and slugs as in steady pipe flow. At higher amplitudes, helical disturbances begin to dominate in a band of intermediate Wommersly number $4 \lesssim Wo \lesssim 18$ which progressively widens toward larger Wo as the oscillatory Reynolds number Re_o is increased. Their dynamics is reminiscent of the Orr-mechanism, however, as the perturbations change their tilt angle, they travel radially inward. This mechanism is most efficient for $Wo \approx 7$, where the maximum amplification exhibits a sharp peak. Remarkably, the maximum gain increases exponentially with the oscillatory Reynolds number (see figures 3, 4 and 6), which is in stark contrast to the Re_s^2 scaling of the classic disturbance.

For the specific case of oscillatory flow ($A \to \infty$), our results are in qualitative agreement with the transient growth analysis of Biau (2016) for oscillatory Stokes flows over a flat plate. In both cases, the maximum energy gain scales exponentially with the Reynolds number of the Stokes layer Re_δ via an analogous (two-dimensional) Orr-mechanism. A

key difference between oscillatory pipe flow and oscillatory flow over a flat plate is that the former is not solely governed by Re_δ, but also by Wo. In particular, the thickness of the Stokes layer in oscillatory pipe flow scales as Wo^{-1} and at sufficiently low Wo it fills the pipe. Hence, oscillatory pipe flow is only exactly similar to oscillatory flow over a flat plate in the limit $Wo \to \infty$, where curvature effects become negligible (Thomas *et al.* 2012). This convergence can be observed in figure 6(c); axisymmetric disturbances dominate for $Re_\delta \gtrsim 200$ at $Wo = 20$, $Re_\delta \gtrsim 400$ at $Wo = 15$, whereas for $Wo = 10$ helical disturbances dominate even up to $Re_\delta \approx 800$. Note also that the axial wavenumber of the optimal disturbance scaled with δ^{-1} is close to 0.4 in figure 6, which is in excellent agreement with figure 2 of Biau (2016). We suggest that when the Stokes layer becomes thick (here for $Wo \lesssim 9$), the mechanism is hindered and becomes entirely inefficient in the quasi-steady limit (practically for $Wo \lesssim 3$, see figure 5). Indeed, in the quasi-steady limit ($Wo \to 0$) the optimal disturbance is the classic one and the maximum growth scales as $(Re_s + Re_o)^2$.

In this paper, we considered linear transient growth of disturbances, but transition to turbulence can only be completed and sustained with nonlinear mechanisms. Xu *et al.* (2020) showed that initializing direct numerical simulations with the linear optimal helical disturbance for $(Re_s, A, Wo) = (2200, 0.85, 5.6)$ can trigger turbulent flow patterns as those observed in their experiments (employing different types of disturbances). In addition, transition in experiments of oscillatory pipe flow occur in the sub-critical regime with a transition threshold independent of Wo and scaling solely with Re_δ (with different critical numbers $280 \lesssim Re_\delta \lesssim 550$ depending on the setup, see Sergeev 1966; Merkli & Thomann 1975; Hino *et al.* 1976; Eckmann & Grotberg 1991; Zhao & Cheng 1996). This is consistent with our observation that the maximum disturbance gain depends only on Re_δ and suggests that the transient growth of helical (and axisymmetric) disturbances underlies the transition in oscillatory pipe flow and pulsatile pipe flow at sufficiently high pulsation amplitude.

Acknowledgment

This work was supported by the Deutsche Forschungsgemeinschaft (DFG) in the framework of the research unit FOR 2688 'Instabilities, Bifurcations and Migration in Pulsatile Flows' under grant AV 120/6-1. Baofang Song acknowledges the financial support from the National Natural Science Foundation of China under grant number 91852105.

REFERENCES

Avila, K., Moxey, D., de Lozar, A., Avila, M., Barkley, D. & Hof, B. 2011 The onset of turbulence in pipe flow. *Science* **333**, 192–196.

Barkley, D., Blackburn, H. M. & Sherwin, S. J. 2008 Direct optimal growth analysis for timesteppers. *Int. J. Numer. Meth. Fluids* **57**, 1435–1458.

Biau, D. 2016 Transient growth of perturbations in Stokes oscillatory flows. *J. Fluid Mech.* **794**, R4.

Blackburn, H. M., Sherwin, S. J. & Barkley, D. 2008 Convective instability and transient growth in steady and pulsatile stenotic flows. *J. Fluid Mech.* **607**, 267–277.

Boyd, J. P. 1983 The continuous spectrum of linear couette flow with the beta effect. *J. Atmos. Sci.* **40** (9), 2304–2308.

Brandt, L. 2014 The lift-up effect: The linear mechanism behind transition and turbulence in shear flows. *Eur. J. Mech. B/Fluids* **47**, 80–96.

Chiu, J.-J. & Chien, S. 2011 Effects of disturbed flow on vascular endothelium: pathophysiological basis and clinical perspectives. *Physiol. Rev.* **91** (1), 327–387.

Eckmann, D. M. & Grotberg, J. B. 1991 Experiments on transition to turbulence in oscillatory pipe flow. *J. Fluid Mech.* **222**, 329–350.

Farrell, B. F. 1988 Optimal excitation of perturbations in viscous shear flows. *Phys. Fluids* **31**, 2093–2102.

Feldmann, D. & Wagner, C. 2012 Direct numerical simulation of fully developed turbulent and oscillatory pipe flows at $Re_\tau = 1440$. *J. Turbul.* **13** (32), 1–28.

Feldmann, D. & Wagner, C. 2016 On the influence of computational domain length on turbulence in oscillatory pipe flow. *Int. J. Heat Fluid Fl.* **61**, 229–244.

Hino, M., Sawamoto, M. & Takasu, S. 1976 Experiments on transition to turbulence in an oscillatory pipe flow. *J. Fluid Mech.* **75**, 193–207.

Kleinstreuer, C & Zhang, Z 2010 Airflow and particle transport in the human respiratory system. *Annu. Rev. Fluid Mech.* **42**, 301–334.

Ku, D. N. 1997 Blood flow in arteries. *Annu. Rev. Fluid Mech.* **29** (1), 399–434.

Maretzke, S., Hof, B. & Avila, M. 2014 Transient growth in linearly stable Taylor-Couette flows. *J. Fluid Mech.* **742**, 254–290.

Merkli, P. & Thomann, H. 1975 Transition to turbulence in oscillating pipe flow. *J. Fluid Mech.* **68**, 567–575.

Meseguer, Á. & Trefethen, L. N. 2003 Linearized pipe flow to Reynolds number 10^7. *J. Comput. Phys.* **186**, 178–197.

Orr, W. 1907 The stability or instability of the steady motions of a perfect liquid and of a viscous liquid. Part II: a viscous liquid. *Proc. R. Irish Acad.* **27**, 69–138.

Reynolds, O. 1883 An experimental investigation of the circumstances which determine whether the motion of water in parallel channels shall be direct or sinuous, and of the law of resistance in parallel channels. *Phil. Trans. R. Soc. Lond.* **174**, 935–982.

Sarpkaya, T. 1966 Experimental determination of the critical Reynolds number for pulsating Poiseuille flow. *J. Fluids Eng.* **88**, 589–598.

Schmid, P. J. & Henningson, D. S. 1994 Optimal energy density growth in hagen–poiseuille flow. *J. Fluid Mech.* **277**, 197–225.

Schmid, P. J. & Henningson, D. S. 2001 *Stability and transition in shear flows*. Springer.

Sergeev, S. I. 1966 Fluid oscillations in pipes at moderate Reynolds numbers. *Fluid Dyn.* **1**, 21–22.

Stettler, J. & Hussain, A. 1986 On transition of the pulsatile pipe flow. *J. Fluid Mech.* **170**, 169–197.

Thomas, C., Bassom, A. P. & Blennerhassett, P. J. 2012 The linear stability of oscillating pipe flow. *Phys. Fluids* **24**, 014106.

Thomas, C., Bassom, A. P., Blennerhassett, P. J. & Davies, C. 2011 The linear stability of oscillatory Poiseuille flow in channels and pipes. *Phil. Trans. R. Soc. A* **467**, 2643–2662.

Tsigklifis, K. & Lucey, A. D. 2017 Asymptotic stability and transient growth in pulsatile Poiseuille flow through a compliant channel. *J. Fluid Mech.* **820**, 370–399.

Xu, D. & Avila, M. 2018 The effect of pulsation frequency on transition in pulsatile pipe flow. *J. Fluid Mech.* **857**, 937–951.

Xu, D., Varshney, A., Ma, X., Song, B., Riedl, M., Avila, M. & Hof, B. 2020 Nonlinear hydrodynamic instability and turbulence in pulsatile flow. *Proc. Natl. Acad. Sci. U. S. A.* **117** (21), 11233–11239.

Xu, D., Warnecke, S., Song, B., Ma, X. & Hof, B. 2017 Transition to turbulence in pulsating pipe flow. *J. Fluid Mech.* **831**, 418–432.

Zhao, T. S. & Cheng, P. 1996 Experimental studies on the onset of turbulence and frictional losses in an oscillatory turbulent pipe flow. *Int. J. Heat Fluid Flow* **17** (4), 356–362.